Pergamon

Geochimica et Cosmochimica Acta, Vol. 65, No. 7, pp. 1015–1023, 2001
Copyright © 2001 Elsevier Science Ltd
Printed in the USA. All rights reserved
0016-7037/01 $20.00 + .00

PII S0016-7037(00)00593-7

Sorption of As(V) on green rust ($Fe_4(II)Fe_2(III)(OH)_{12}SO_4 \cdot 3H_2O$) and lepidocrocite ($\gamma$-FeOOH): Surface complexes from EXAFS spectroscopy

SIMON R. RANDALL, DAVID M. SHERMAN,* and K. VALA RAGNARSDOTTIR
Department of Earth Sciences, University of Bristol, Bristol BS8 1RJ, UK

(*Received December* 16, 1999; *accepted in revised form October* 11, 2000)

Abstract—Green rust ($Fe_4(II)Fe_2(III)(OH)_{12}SO_4 \cdot 3H_2O$) is an intermediate phase in the formation of iron (oxyhydr)oxides such as goethite, lepidocrocite and magnetite; current thinking is that it occurs in many soil and sediment systems. Green rust has been shown to reduce sorbed selenate and nitrate and, therefore, might presumeably reduce sorbed arsenate to the more toxic and mobile As(III) species. We have investigated the mechanism of As(V) sorption onto green rust and its fate during oxidation of green rust to lepidocrocite. EXAFS spectroscopy was used to determine the As speciation and coordination environment. We find that As(V) is not reduced to the more mobile and toxic As(III) form following equilibrium with green rust for 24 h. It remains adsorbed as $(AsO_4)^{3-}$ by forming inner-sphere surface complexes. The same result is obtained whether As(V) is added prior to or after green rust nucleation. Two different inner sphere surface complexes are resolved: one results from edge-sharing between AsO_4 and FeO_6 polyhedra while the second results from and double-corner sharing between AsO_4 tetrahedra and adjacent FeO_6 polyhedra. During the oxidation of green rust to lepidocrocite, the $(AsO_4)^{3-}$ remains preferentially bound to green rust and only sorbs onto lepidocrocite when all of the green rust has been oxidized. Sorption onto lepidocrocite occurs via an inner-sphere complex resulting from bidentate corner sharing between AsO_4 tetrahedra and adjacent FeO_6 octahedra. *Copyright © 2001 Elsevier Science Ltd*

1. INTRODUCTION

Aqueous speciation of arsenic is dominated by the As(V) oxyanions $H_2AsO_4^-$ and $HAsO_4^{2-}$ under oxidising conditions (Grossl et al., 1997) and the neutral As(III) species $H_3AsO_3^0$ under more reducing conditions (Masscheleyn, 1991; Grossl et al., 1997) (Fig. 1). The As(III) species is far more toxic (Ferguson and Gavis, 1972), soluble and mobile (Pierce and Moore, 1982) than the arsenate species which are strongly adsorbed by iron oxyhydroxides (Livesey and Huang, 1981; Aggett and O'Brien, 1985; Moore et al., 1988; Belzile and Tessier, 1990; Fuller et al., 1993; Waychunas et al., 1993; Sullivan and Aller, 1996; Sun and Doner, 1996).

'Green rusts' are green-blue Fe(II)-Fe(III) hydroxides which were first identified as corrosion products of steel and iron water pipes (Stampfl, 1969). They are postulated to be intermediate phases in the formation of iron (oxyhydr)oxides such as goethite, lepidocrocite and magnetite via the oxidation of Fe(II) under reducing and weakly acidic to weakly alkaline conditions (Schwertmann and Fechter, 1994). Importantly, they can also form during the reductive dissolution of existing Fe(III) (oxyhydr)oxides (Hansen et al., 1994; Schwertmann and Fechter, 1994), and Fredrickson et al. (1998) have shown that green rust formation can occur during dissimilatory reduction of hydrous ferric oxide by a groundwater bacterium. The mottling often observed in gleyed soil horizons and the grey-green colour in the uppermost layers of some lake and marine sediments has been attributed to the presence of mixed-valence minerals such as green rust (Buurman, 1980; Newman, 1987). However, green rust has only been positively identified in recent times (Trolard et al., 1997) because the extreme air-sensitivity of this mineral has made its isolation and characterisation difficult. Upon exposure to air, green rust is oxidized to either lepidocrocite (γ-FeOOH) or magnetite (Fe_3O_4) depending on the rate and pH of oxidation.

Green rust minerals possess the pyroaurite-sjögrenite structure consisting of sheets of $Fe(II)(OH)_6$ in which some of the Fe(II) is replaced by Fe(III) (Taylor, 1973; Brindley and Bish, 1976; Allman, 1968) (Fig. 2). This results in a positive layer charge which is balanced by the inclusion of anions such as Cl^-, CO_3^{2-}, and SO_4^{2-} between the layers (Feitknecht and Keller, 1950; Bernal et al., 1959; Stampfl, 1969; Brindley and Bish, 1976). The resulting green rusts are termed GR1(Cl^-), GR2(CO_3^{2-},), and GR2(SO_4^{2-}). Sulphate and carbonate are the most commonly reported interlayer anions in nature, and the sulphate form of green rust has the general formula $Fe_y^{(II)}Fe_x^{(III)}(OH)_{3x+2y-2z}(SO_4)_z$ (Schwertmann and Fechter, 1994).

Green rusts may be important for trace metal mobility in the environment because of their high reactive surface area and their potential to reduce metal species such as As(V) and Cr(VI). The reduction of As(V) following adsorption on green rust would probably lead to the desorption of the more toxic As(III) because this is less strongly adsorbed than As(V) (Bowell, 1994). To date, relatively few studies of the interaction of trace groundwater components with green rust have been performed. Myneni et al. (1997) observed that Se(VI) was reduced directly to Se(0) following adsorption, and more rapidly to Se(0) via a Se(IV) intermediate following co-precipitation into the interlayer anion sites. Hansen et al., (1994; 1996) have also shown that sulphate green rust is capable of reducing nitrate to ammonium. Importantly, the rates of abiotic selenium and nitrate reduction by green rust were comparable to those achieved via microbial pathways (Myneni et al., 1997).

*Author to whom correspondence should be addressed (dave.sherman@bris.ac.uk).

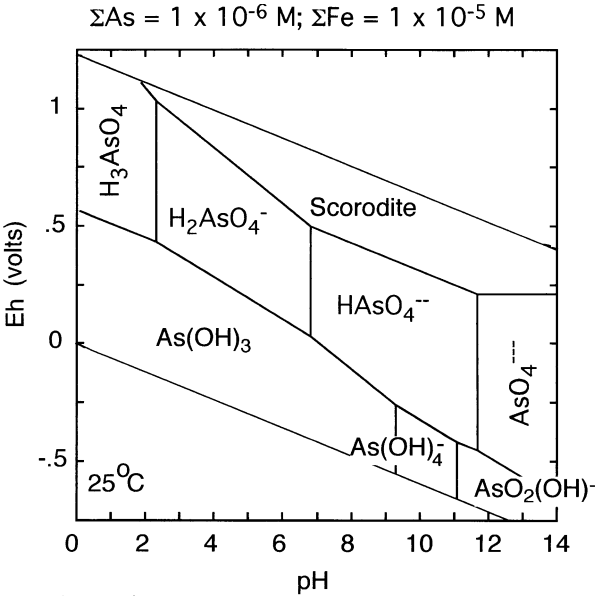

Fig. 1. Eh-pH diagram for As species.

The goal of this work is to understand the mechanism of sorption of As(V) on green rust phases and the fate of sorbed arsenic during the oxidation of green rust to lepidocrocite under the conditions expected near the oxic-anoxic boundary.

2. EXPERIMENTAL

2.1. General

All reagents used in this study were analytical grade and labware was acid-washed. An Orion model 720A meter was used to make pH measurements with a Willhelm-type reference electrode–glass pH electrode pairing (both from both Sentek Ltd.). Calibration ± 0.05 pH units was achieved at room temperature with constantly stirred Whatman NBS grade buffers. The As(V) stock solution was prepared from $Na_2HAsO_4 \cdot 7H_2O$ and was stored at 4°C in a closed amber-coloured HDPE bottle.

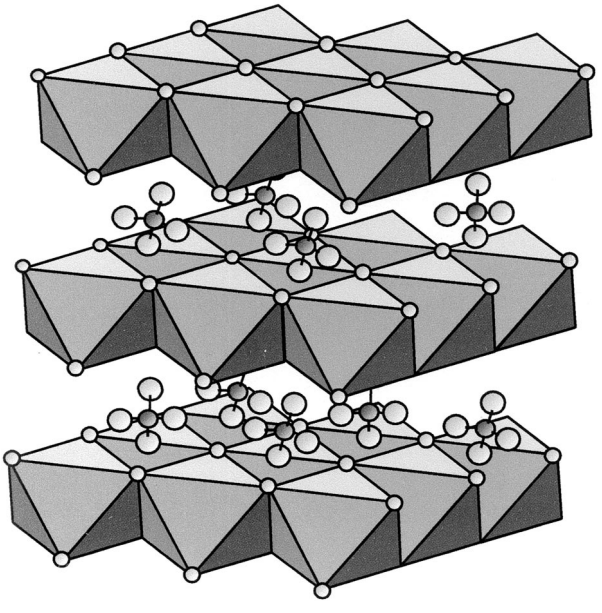

Fig. 2. The crystal structure of green rust compounds consists of layers of Fe(II)(OH)6 in which some of the Fe(II) is replaced by Fe(III). These alternate with layers of anions (SO_4^{2-}, CO_3^{2-} and Cl^-) and water which bind the $Fe(OH)_6$ layers via hydrogen bonding. The pyroaurite-type structure, which green rust shares, is shown here (Allmann, 1968).

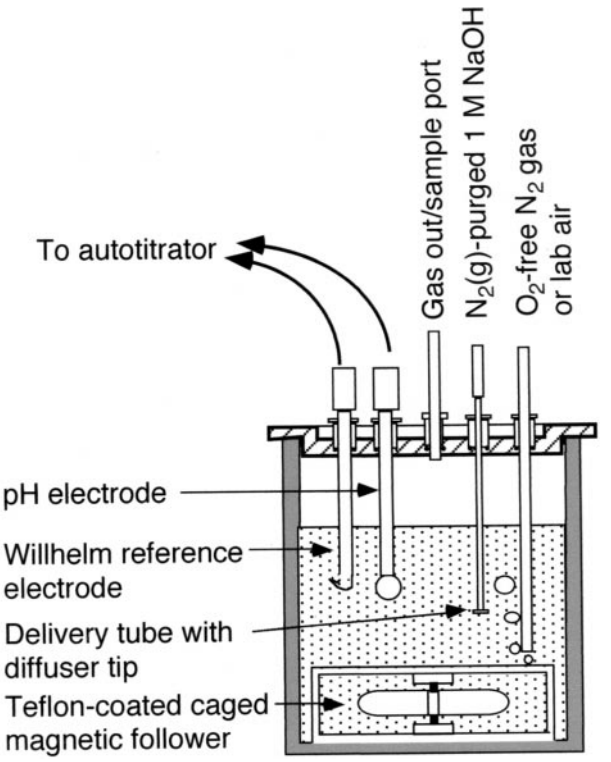

Fig. 3. Reaction vessel used to prepare samples of green rust to which As(V) was added after formation ('As-GR' sample series) and before nucleation ('As-GRCO' series). The total volume of the reaction vessel was 500 mL, and it was wrapped in aluminium foil at all times to exclude light which may have otherwise caused unwanted photoredox reactions. The 1 mol/L NaOH was supplied by a Metrohm 718 pH-stating titrator; it was stored in a plastic reagent bottle before delivery to the reaction vessel to prevent possible leaching of silica from the walls of a glass reagent bottle.

2.2. Reaction of As(V) with Green Rust

2.2.1. Preparation of green rust with adsorbed As(V) ('AS-GR' sample series)

The method of Schwertmann and Fechter (1994) was followed to prepare sulphate green rust ($GR2(SO_4^{2-})$) with the expected approximate bulk formula $Fe^2_{(II)}Fe^{(III)}(OH)_5(SO_4)$. Light was excluded from all samples during preparation and analysis to prevent unwanted photoredox reactions. Sample preparation took place in a 500 mL straight-sided polythene beaker. This contained a magnetic follower and was capped by an airtight PVC lid with holes for pH electrodes, gas inlet/outlet ports and sample ports (Fig. 3).

Initially, 370 mL of MilliQ water was added to the beaker and purged with $N_2(g)$ for 48 h to remove dissolved oxygen before the addition of 20.57 g of $FeSO_4 \cdot 7H_2O$. The resulting light green solution was continually purged with $N_2(g)$ whilst the pH was raised from an initial value of ~3.4 to pH 7.0 over a 15 min period by the addition of CO_2/N_2-free 1.0 mol/L NaOH from a Metrohm 718 pH-stat titrator. Once pH 7.0 was reached, the $N_2(g)$ flow was replaced with laboratory air supplied by a small pump via an open ended 4 mm ID glass tube. The light green solution started to darken in colour and become more

turgid as soon as air flow began, and passed through consecutive dark green-blue, ochre-green and finally bright orange stages over a period of approximately 6 h. Because the oxidation/hydrolysis reaction liberates protons, the 718 titrator was required to constantly add 1.0 mol/L NaOH throughout the reaction to maintain pH at 7.0 ± 0.1. The rate of base addition was high for the first ~100 min of reaction (~0.6 mL/min), but subsequently decreased to a much lower and constant value of ~0.03 mL/min.

The dark green suspension was first sampled after 50 min, and 14.7 mL of a 1340 ppm As(V) stock solution was then added. Further samples were collected periodically throughout the course of the 18 h reaction. Sampling was achieved with 20 mL plastic syringes fitted with 50 mm long needles that were used to pierce rubber septa in the sample ports (Fig. 3). The suspension collected in this way was transferred immediately to 50 mL screw-top polypropylene copolymer centrifuge tubes that were filled to the brim with no trapped air. These were stored in the dark at room temperature for the duration of the reaction and then centrifuged after the last sample had been collected. This allowed the arsenic in solution ample time (12–18 h) to equilibrate with the solid phase.

All of the green rust adsorption samples were frozen immediately after separation from the supernatant to prevent oxidation during storage. This was achieved by briefly immersing the centrifuge tubes in which they were contained in liquid nitrogen. Note that the concentration of dissolved iron was also measured by ICP-AES in all samples to establish the relationship between levels of dissolved arsenic and iron as a function of reaction time.

X-ray diffraction was used to determine the mineralogy of all samples. The XRD slides were prepared by air-drying a glycerol-based suspension of each sample onto small glass discs. The glycerol-based suspension was generated by quickly mixing a drop of each green rust sample with a small amount of glycerol. This resulted in a viscous paste which protected the air-sensitive samples against oxidation during XRD analysis (Hansen et al., 1994). Note that there was no significant difference in diffraction patterns collected from a fully oxidised sample with and without the glycerol matrix. Comparison of the relative intensity of observed green rust and lepidocrocite diffraction peaks allowed a qualitative assessment of the rate of green rust oxidation.

The reproducibility of the green rust preparation method was verified by generating a set of duplicate samples and analysing them by XRD. The results from both sets of samples were in good agreement.

2.2.2. Preparation of green rust with coprecipitated As(V) ('As-GRCO' sample series)

A series of green rust samples were prepared and progressively oxidised in the presence of As(V) using exactly the same method that was used to prepare the 'As-GR' sample series, with the exception that the As(V) stock solution was added before, rather than after, the nucleation of green rust from solution. Samples were first collected 1 h after green rust formation commenced, and then periodically throughout the 18 h reaction. Sample collection and treatment was exactly the same as detailed above.

2.2.3. As(V) sorption on lepidocrocite ('As-LEPID')

Lepidocrocite was prepared by the oxidation/hydrolysis of a ferrous chloride solution at pH 6.7–6.9 (Schwertmann and Cornell, 1991). The bright orange precipitate was collected by centrifugation, cleaned by dialysis against MilliQ water and stored as a refrigerated 20 g L^{-1} stock suspension before use. X-ray powder diffraction of a randomly oriented powder sample was used to confirm the identity and purity of the crystalline product. Additionally, its surface area (88 ± 3 m^2g^{-1}) was determined by BET surface area analysis following 12 h of outgassing with N_2(g). Transmission electron microscopy showed the crystallites to measure approximately 300 nm long by 120 nm wideand displayed the platy morphology that is characteristic of γ-FeOOH.

Aliquots of the lepidocrocite stock suspension were air dried at ~50°C for 48 h. The dry material was then crushed with an agate mortar and pestleand 0.50 g of the resulting fine powder was weighed out into 370 mL of MilliQ water with a 0.1 mol/L $NaClO_4$ background electrolyte. The added lepidocrocite was thoroughly dispersed by a combination of stirring and treatment in an ultrasound bath, and was allowed to re-hydrate over a 24 h period. Subsequently, 1.12 mL of a 1340 ppm stock solution was added to the lepidocrocite suspensions with stirring. The lepidocrocite suspension was equilibrated at pH 7.0 ± 0.05 by the addition of 0.1 mol/L NaOH from a Metrohm 718 pH stat titrator under ambient temperature and atmospheric conditions for 24 h.

2.3. EXAFS Data Collection and Analysis

2.3.1. Data collection

EXAFS data were collected at the CLRC Synchrotron Radiation Source at Daresbury Laboratory, U.K. Spectra were collected at the arsenic K-edge (11.8667 keV) on station 16.5. Samples were kept at 77 K during EXAFS measurements to minimise the risk of oxidation. Station 16.5 is equipped with a water cooled, harmonic rejecting double crystal Si (311) monochromator and a 1.2m long plane mirror which is bent to provide vertical focusing. Because the focusing mirror minimised higher harmonics in the EXAFS spectra, it was not necessary to detune the monochromator during data collection. The storage ring energy was 2.0 GeV and the beam current varied between 130 and 240 mA during data collection. Each adsorption sample was presented to the X-ray beam as a viscous paste held by Sellotape in a 2 mm-thick Teflon slide with a 4 × 15 mm sample slot. EXAFS data were collected from the green rust and lepidocrocite samples during four to six fluorescence mode scans using an Ortec 30-element solid state detector. EXAFS data were also collected for scorodite ($FeAsO_4 \cdot 4H_2O$) in three room temperature transmission mode scans.

2.3.2. Data analysis

EXAFS data reduction was performed using Daresbury Laboratory software (EXCALIB and EXBACK) (Dent and Mosselmans, 1992). EXCALIB was used to calibrate from monochromator position (millidegrees) to energy (eV) and to average multiple spectra from individual samples. EXBACK was used to define the start of the EXAFS oscillations and perform background subtraction.

The exact curved wave theory EXAFS analysis program EXCURV98 (Gurman et al., 1984; 1986; Joyner et al., 1987; Gurman, 1988; Binsted et al., 1991) was used to analyse the EXAFS data. This process involved the comparison of experimental data with theoretical EXAFS oscillations that were derived by EXCURV98 from model clusters. The geometry of these clusters was based on knowledge of the likely arsenic coordination environment in each sample. In all cases, the cluster that provided the closest initial fit underwent least squares refinement of: Debye-Waller factor, number of atoms per shell, As-X distance, and Fermi energy to improve the fit between its theoretical oscillations and the experimental data. The model clusters initially consisted of only one atomic shell. Successive shells were added to the theoretical model until each significant peak in the Fourier transform of the EXAFS data was accounted for. Statistical tests (Joyner et al., 1987) were performed to ascertain the significance of each new atomic shell, and only those which improved the fit between theory and experiment at the 99% level of confidence were retained.

The phase-shift functions used in the curve fitting were derived by ab initio methods in EXCURV98 using Hedin-Lundqvist potentials (Hedin and Lundqvist, 1969) and von Bart ground states. Our use of theoretical values is justified by good agreement between the structures of scorodite derived from our EXAFS data using theoretical phase-shift functions and the published data from these minerals (Kitahama et al., 1975).

3. RESULTS AND DISCUSSION

3.1. Surface Complexation of As(V) on Lepidocrocite

After 24 h at pH = 7.0, the concentration of As sorbed on lepidocrocite was 0.27 wt %. Assuming a surface site density of 1.58 sites/nm, this corresponds to a 27% surface loading. EXAFS spectra (Fig. 4) of As-LEPID sample show that there is an inner sphere complex of $(AsO_4)^{3-}$ with an Fe-As distance of

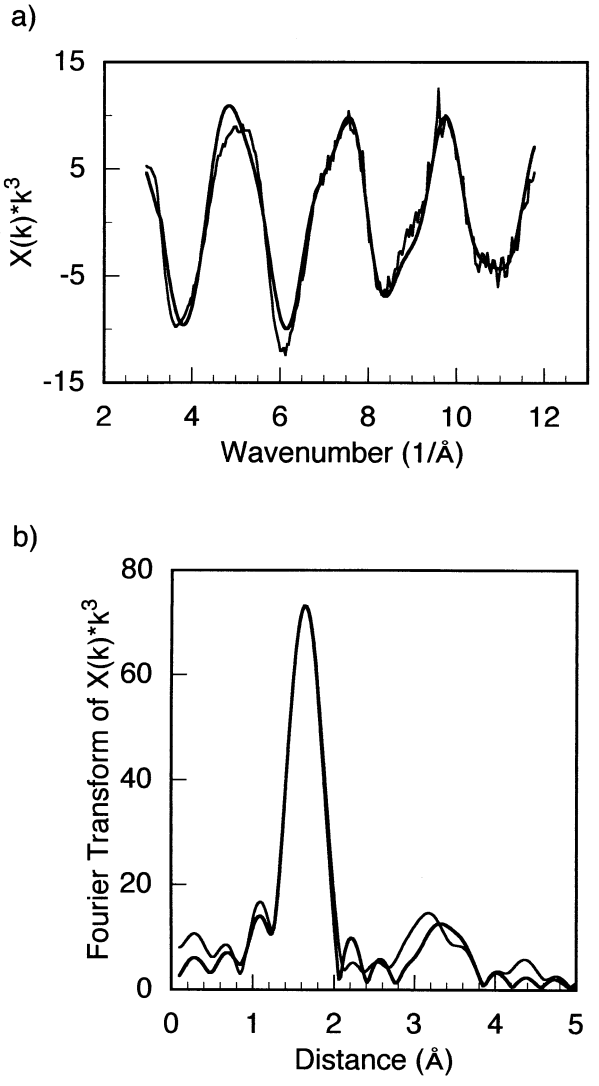

Fig. 4. (a) EXAFS spectra and its Fourier transform (b) of AsO_4 sorbed onto lepidocrocite (As-LEPID).

3.32 Å with 1.7 Fe atoms near the As. This is interpreted as a bidentate double corner-sharing arrangement on the lepidocrocite (001) and (100) surface sites (Fig. 5). Other surface oxygens on lepidocrocite should be less reactive insofar as they have a complete (or nearly complete) coordination environment. In particular, the (010) surface hydroxyls have a complete coordination environment and appear to be very unreactive. We cannot find evidence for single-edge sharing and monodentate complexes of $(AsO_4)^{3-}$ on lepidocrocite; such surface complexes have been found for $(AsO_4)^{3-}$ on goethite (Manceau, 1995; Waychunas et al., 1995).

3.2. The Interaction of As(V) with Green Rust

3.2.1. Chemical observations from the interaction of As(V) with green rust

Levels of dissolved iron and arsenic recorded during the growth and oxidation of a series of green rust samples with

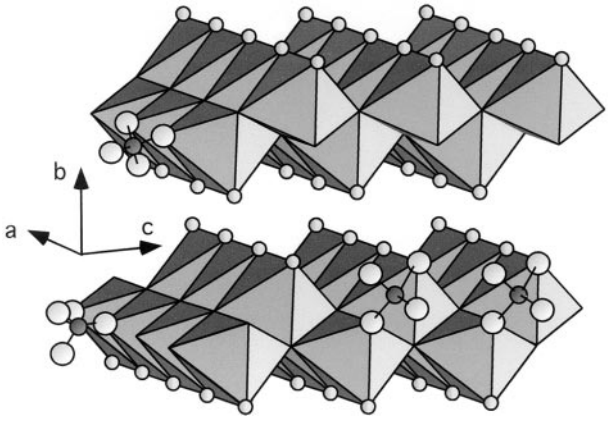

Fig. 5. Inferred inner sphere surface complexes of $(AsO_4)^{3-}$ on lepidocrocite based on EXAFS results.

As(V) added after ('As-GR' series) and before ('As-GRCO' series) are shown in Figure 6. Initial levels of dissolved iron are high in both cases, but represent only 40 to 50% of total iron in the system (11200 ppm if all dissolved). By comparison, initial levels of dissolved arsenic are relatively low; only 6 to 8% of total available arsenic remains in solution one hour after the start of the reaction. This suggests that even when 40 to 50% of total iron is in solution, that which is in a solid form (as green rust) is capable of sorbing 92 to 94% of available arsenic.

Arsenic concentrations remained very low in both series following the first 3 to 4 h of reaction, and ultimately fell below detectable limits. This suggests that As(V) was not reduced to As(III) by the green rust. If it had been, dissolved arsenic levels would have been expected to remain measurable and possibly even increase because As(III) is not as strongly adsorbed as As(V) (Bowell, 1994).

3.2.2. X-ray diffraction results from the interaction of As(V) with green rust

The XRD results from the 'As-GR' sample series are shown in Figure 7a. The characteristic (001), (002) and (003) lines of sulphate green rust (GR2(SO_4^{2-})) can be clearly seen in the data from sample As-GR1. These lines correspond to crystallographic plane spacings of 11.2 Å, 5.58 Å and 3.77 Å (Vins et al., 1987). All other peaks in As-GR1 can also be assigned to GR2(SO_4^{2-}), and there is no evidence for the presence of magnetite (Fe_3O_4). The (001), (002) and (003) peaks become slightly more intense and sharper over the first 4.5 h of oxidation (up to As-GR5) but are absent after 6.0 h (As-GR6). A similar pattern is observed for other less intense green rust peaks such as the (100), (101) and (103). These observations suggest that whilst green rust is being consumed by oxidation, that which remains becomes increasingly crystalline as it ages.

After 3.2 h of oxidation (As-GR4), the (100) and (120) peaks of lepidocrocite start to develop. Since they co-exist with the remaining green rust peaks and there is no evidence for an intermediate phase, it seems likely that green rust oxidises directly into lepidocrocite. Other lepidocrocite peaks, such as the (031) and (051, 200), also grow strongly at the same time as the (100) and (120) peaks.

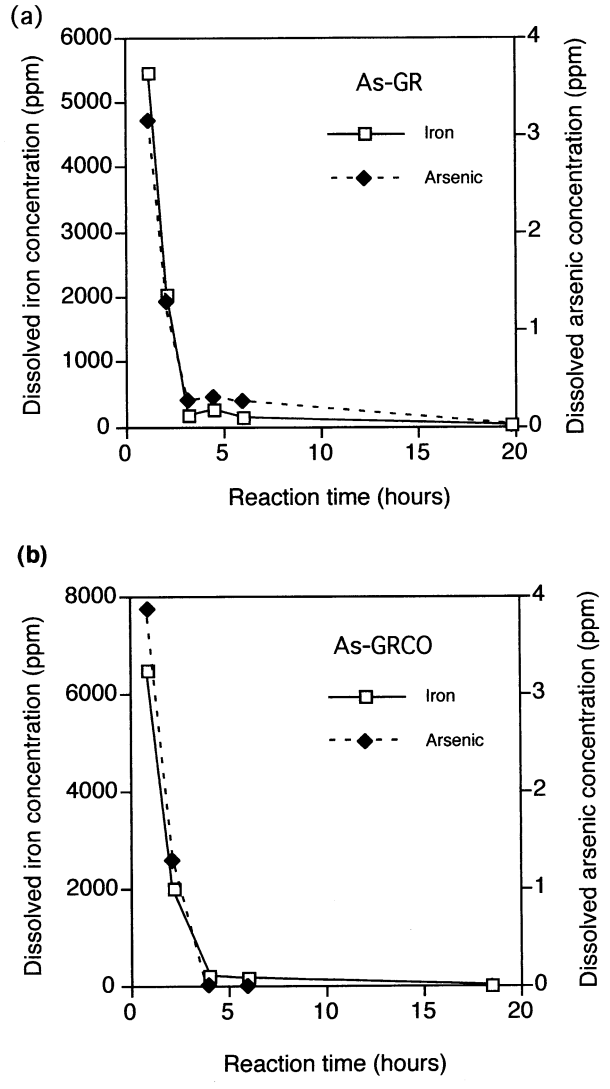

Fig. 6. (a) Changes in dissolved iron and arsenic concentrations during the formation and oxidation of green rust with adsorbed As(V) ('As-GR' sample series). (b). Changes in dissolved iron and arsenic concentrations during the formation and oxidation of green rust that was nucleated in the presence of As(V) ('As-GRCO' sample series).

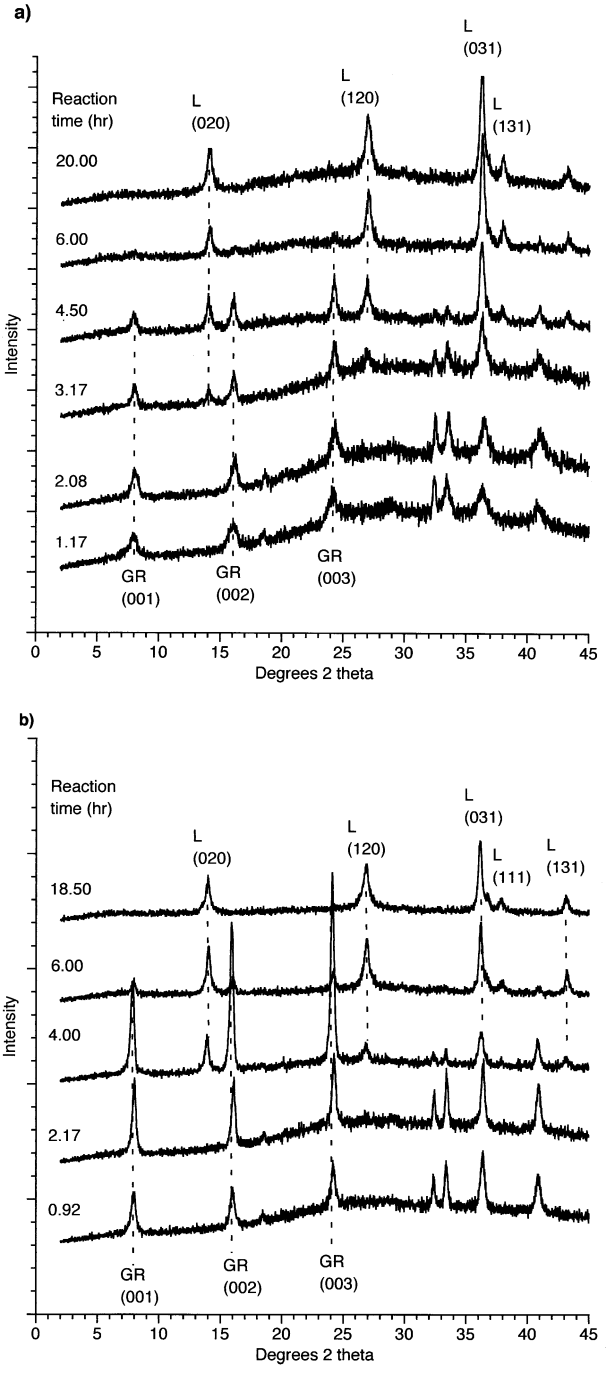

Fig. 7. (a) XRD results from the progressive oxidation of green rust with adsorbed As(V) ('As-GR') to lepidocrocite at pH 7 ± 0.05. Green rust and lepidocrocite peak indexing from Vins et al. (1987) and JCPDS card 8 to 98, respectively. (b) XRD results from the progressive oxidation at pH 7 ± 0.05 of green rust that was nucleated in the presence of As(V) ('As-GRCO'). Green rust and lepidocrocite peak indexing from Vins et al. (1987) and JCPDS card 8 to 98, respectively.

After 6.0 h of oxidation, all green rust has been oxidised. Thereafter, the lepidocrocite peaks simply become more intense, presumably as a result of an increase in crystallinity with ageing. There is no evidence for the development of other mineral phases. Although the peaks in As-GR7 are well defined, they are two to three times less intense than those recorded from a pure lepidocrocite XRD standard (data not shown). This suggests that the material in As-GR7 is not highly crystalline and that sorbed As(V) prevents recrystallization as is the case for sorbed As(V) on ferrihydrite (Waychunas et al., 1993; Waychunas et al., 1996).

The XRD results for the 'As-GRCO' sample series (Fig. 7b) are very similar to those from the 'As-GR' series of samples; all peaks in As-GRCO1 can be assigned to sulphate green rust whilst all those in the final oxidation product (As-GRCO5) can be assigned to lepidocrocite. Increases in diffraction peak intensity suggest that the green rust is becoming more crystalline as it ages, and the coexistence of lepidocrocite and green rust diffraction peaks between 4.00 and 6.00 h of oxidation indicates that green rust is oxidising directly into lepidocrocite.

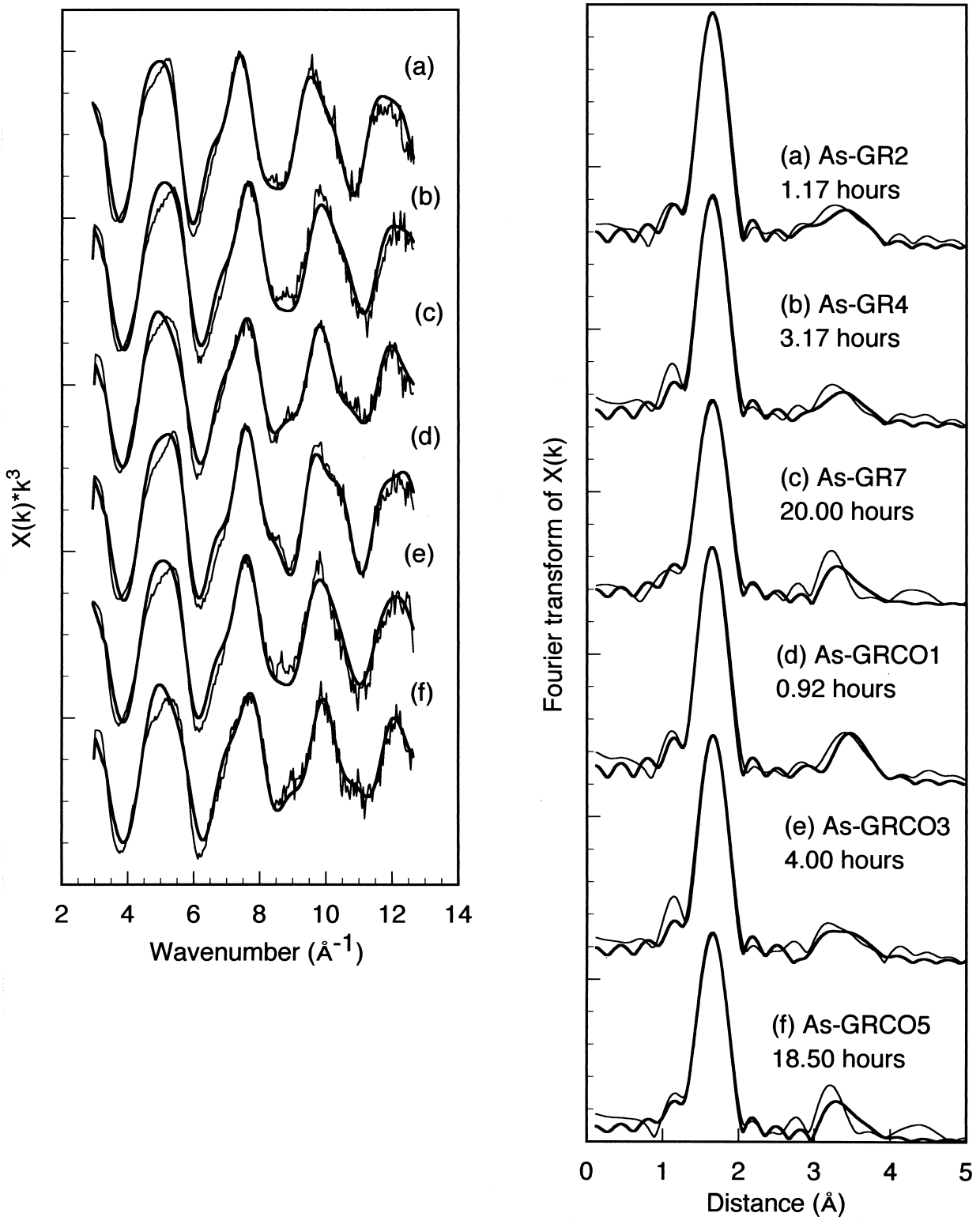

Fig. 8. EXAFS spectra (left) and the Fourier transforms of the spectra (right) of arsenic which was added after (a to c) and before (d to f) nucleation of green rust. Spectra show the change in arsenic coordination during the oxidation of green rust to lepidocrocite. Before the formation of lepidocrocite, As atoms occur as $(AsO_4)^{3-}$ anions with iron neighbors at 2.88 to 2.95 Å and 3.42 to 3.47 Å. These are consistent with single edge- and double corner sharing of $(AsO_4)^{3-}$ on a ferrous hydroxide sheet (Fig. 9). Importantly, there is no evidence for the reduction of As(V) to As(III) on green rust. After the transformation of green rust to lepidocrocite (samples c and f) the As atoms have just one iron shell at 3.36 Å; this iron shell is due to double corner sharing between $(AsO_4)^{3-}$ with surface ferric hydroxide polyhedra on lepidocrocite

Table 1. EXAFS results from As (V) on green rust, As(V)-green rust coprecipitate and As on lepidocrocite samples.

Sample	Oxidation time (hr)	R_{As-O}	CN_O $2\sigma^2$ O	R_{As-Fe2}	CN_{Fe2} $2\sigma^2$ Fe 1	R_{As-Fe2}	CN_{Fe2} $2\sigma^2$ Fe 2	R factor
As-GR2	1.17	1.69	3.9	2.90	1.1	3.42	1.7	20.7
			0.004		*0.019*		*0.011*	
As-Gr4	3.17	1.69	4.1	2.91	0.9	3.42	1.5	25.2
			0.005		*0.019*		*0.011*	
As-GR7	20.00	1.69	3.8	3.36	1.6	—	—	22.0
			0.006		*0.011*			
As-GRCO1	0.92	1.69	4.0	2.88	0.8	3.45	2.5	22.0
			0.004		*0.019*		*0.012*	
As-GRCO3	4.00	1.70	4.0	2.95	0.7	3.47	1.9	25.7
			0.005		*0.019*		*0.017*	
As-GRCO5	18.50	1.69	3.9	3.36	1.5	—	—	27.2
			0.006		*0.009*			
As-LEPID (0.3 wt%)		1.69	4.0	3.32	1.7	—	—	22.0
			0.003		0.011			

CN_x is number of atoms in a shell at distance R_x (Å) from the central cadmium atom. $2\sigma_x^2$ (Å)^2) is the associated Debye-Waller factor. The *R* factor gives a measure of the agreement between experimental and theoretical EXAFS curves. $R < 20\%$ indicates a very good fit whereas $R \leq 40\%$ is acceptable.

3.2.3. EXAFS results from the interaction of As(V) with green rust

The arsenic K-edge EXAFS results from the 'As-GR' and 'As-GRCO' series of samples are shown in Figure 8 and summarised in Table 1. The most striking and important feature of these EXAFS results is that arsenic exists as arsenate (4 oxygen atoms at an As-O distance of 1.69–1.70 Å) in all samples. There is no evidence to suggest the formation of the more mobile As(III) species, which is characterised by a shell of 3.0 oxygen atoms at an As-O distance of 1.79 Å (Manning et al., 1998). The first two samples from both the 'As-GR' and 'As-GRCO' series have iron shell contributions at 2.88 to 2.95 Å and 3.42 to 3.47 Å. These are consistent with single edge and double corner adsorption on $Fe(II)O_6$ octahedra (Fig. 9). Iron shell coordination numbers fall in the range 0.7 to 2.5. This strongly suggests that As(V) remained adsorbed in surface complexes throughout the formation and oxidation of green rust, and not as a coprecipitate and/or solid solution with iron.

The free energy of formation of green rust with composition $Fe_4^{II}Fe_2^{III}(OH)_{12}SO_4 \cdot 3H_2O$ is -1046.8 kcal/mole (Hansen et al., 1994). Using this, together with thermodynamic data tabulated in Shock and Helgeson (1988), we estimate the free energy of the reaction

$$H_2AsO_4^-(aq) + 0.5Fe_4^{II}Fe_2^{III}(OH)_{12}SO_4{\cdot}3H_2O = H_2AsO_3^- + 0.5SO_4^{2-} + 3\gamma\text{-FeOOH} + 5/2H_2O + H^+ \quad (1)$$

to be -22.74 kJ/mol giving a pK of -3.98. The absence of reduction of As(V) when sorbed on green rust implies that the free energy (activity) of $H_2AsO_4^-$ is strongly decreased by formation of a stable surface adsorption complex by AsO_4^- onto the green rust. Since both the 'As-GR' and 'As-GRCO' samples were equilibrated at room temperature for no more than 24 h, it is possible that As(V) reduction did not occur for kinetic reasons. Unfortunately, this cannot be proven because no kinetic data for the reaction between solid phase Fe(II) and aqueous As(V) has been published. The absence of As(III) cannot be explained by its oxidation during EXAFS analysis since there were never any differences between multiple EXAFS spectra that were collected from any one given sample over a period of hours. Manning et al. (1998) have previously proven this point during their EXAFS and XANES analysis of As(III) adsorbed on goethite. Moreover, our spectra were collected at 77 K.

After the complete oxidation of green rust to lepidocrocite, the As coordination environment is now characterised by just one As-Fe interaction (Fig. 8 c,f; Table 1). The As-Fe distance of 3.36 Å suggests that adsorption occurs via bidentate double corner sharing between the apices of adjacent $Fe(III)O_6$ octahedra (Fig. 5). The coordination environment observed in As-GR7 and As-GRCO5 is identical to that obtained when As(V) was directly sorbed onto lepidocrocite.

The XRD results clearly show that lepidocrocite was coexisting with green rust when both As-GR4 and As-GRCO3 were collected. Consequently, it is noteworthy that the EXAFS results from these two samples suggest adsorption on Fe(II) (oxyhydr)oxide (green rust) rather than Fe(III) (oxyhydr)oxide (lepidocrocite); this observation indicates that green rust oxi-

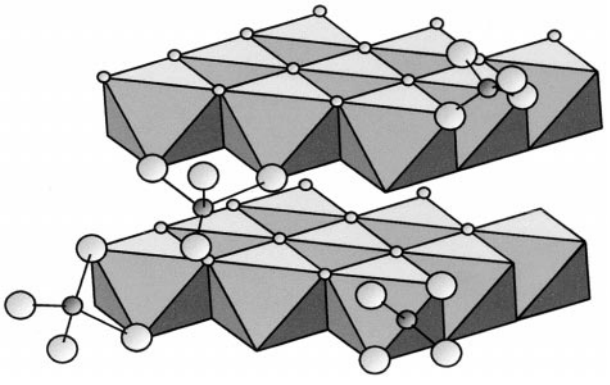

Fig. 9. Proposed inner-sphere surface complexes of $(AsO_4)^{3-}$ on green rust showing both edge-sharing (1 Fe neighbor) and corner-sharing (2 Fe neighbors) arrangements.

dation has to occur before arsenic can become adsorbed by lepidocrocite.

4. CONCLUSIONS

Green rust ($Fe_y^{(II)}Fe_x^{(III)}(OH)_{3x+2y-2z}(SO_4)_z$) is a mixed Fe(II)-Fe(III) oxyhydroxide mineral that is thought to occur under the reducing and mildly acidic to mildly alkaline conditions found in reductomorphic soils and certain sedimentary horizons. Consequently, it is likely to be one of the most important Fe(II)-bearing minerals in immature sediments and soils. Green rust has previously been shown to be capable of reducing Se(VI) to Se(0), and nitrate to ammonium. However, green rust does not reduce As(V) to As(III), irrespective of whether arsenic is added before or after green rust formation. Following adsorption on green rust, As(V) persists as surface complexes, even after the oxidation of green rust to lepidocrocite (γ-FeOOH). It is not incorporated into the green rust bulk structure and it does not exchange for sulphate anions in the interlayer sites that are present in green rust.

Acknowledgments—This work was supported by NERC grant no. GR93506 together with direct access time at Daresbury from CLRC. Simon Randall's studentship was supported by British Nuclear Fuels Ltd. (BNFL).

Associate editor: S. J. Traina

REFERENCES

Aggett J. and O'Brien G. A. (1985) Detailed model for the mobility of arsenic in lacustrine sediments based on measurements in Lake Ohakuri. *Env. Sci. Tech.* **19,** 231–238.

Allman R. (1968) The crystal structure of pyroaurite. *Acta Cryst.* **B24,** 972–977.

Belzile N. and Tessier A. (1990) Interactions between arsenic and iron oxyhydroxides in lacustrine sediments. *Geochim. Cosmochim. Acta* **54,** 103–109.

Bernal J. D., Dasgupta D. R., and MacKay A. L. (1959) The oxides and hydroxide of iron and their structural interrelationships. *Clay Min. Bull.* **4,** 15–30.

Binsted N., Campbell J. W., Gurman S. J., and Stephenson P. C. (1991) SERC Daresbury Laboratory EXCURV92 program. Daresbury Laboratory, Warrington, U.K.

Bowell R. J. (1994) Sorption of arsenic by iron oxides and oxyhydroxides in soils. *Appl. Geochem.* **9,** 279–286.

Brindley G. W. and Bish D. L. (1976) Green rust: A pyroaurite type structure. *Nature* **262,** 353.

Buurman P. (1980) Paleosols in the Reading Beds (Paleocene) of Alum Bay, Isle of Wight, U.K. *Sedimentol.* **27,** 593–606.

Dent A. J. and Mosselmans J. F. W. (1992) A guide to EXBACK, EXCALIB, and EXCURV92. Daresbury Laboratory, Warrington, U.K.

Feitknecht W. and Keller G. (1950) Über die dunkel-grünen Hydroxylverbindungen des Eisens. *Z. anorg. allg. Chem.* **262,** 61–68.

Ferguson J. F. and Gavis J. (1972) A review of the arsenic cycle in natural waters. *Water Res.* **6,** 1259–1274.

Fredrickson J. K., Zachara, J. M., Kennedy D. W., Dong H. L., Onstott T. C., Hinman N. W. and Li S. M. (1998) Biogenic iron mineralization accompanying the dissimilatory reduction of hydrous ferric oxide by a groundwater bacterium. *Geochim. Cosmochim. Acta* **62,** 3239–3257.

Fuller C. C., Davis J. A., and Waychunas G. A. (1993) Surface chemistry of ferrihydrite. 2. Kinetics of arsenate adsorption and coprecipitation. *Geochim. Cosmochim. Acta* **57,** 2271–2282.

Grossl P. R., Eick M., Sparks D. L., Goldberg S. and Ainsworth C. C. (1997) Arsenate and chromate retention mechanisms on goethite. 2. Kinetic evaluation using a pressure-jump relaxation technique. *Env. Sci. Tech.* **31,** 321–326.

Gurman S. J. (1988) The small atom approximation theory. *J. Phys. C: Solid State Phys.* **21,** 3699–3717.

Gurman S. J., Binsted N., and Ross I. (1984) Single scattering rapid curved wave theory. *J. Phys. C: Solid State Phys.* **17,** 143–151.

Gurman S. J., Binsted N., and Ross I. (1986) Multiple scattering rapid curved wave theory. *J. Phys. C: Solid State Phys.* **19,** 1845–1861.

Hansen H. C. B., Borggaard O. K., and Sorensen J. (1994) Evaluation of the free energy of formation of Fe(II)-Fe(III) hydroxide-sulfate (green rust) and its reduction of nitrite. *Geochim. Cosmochim. Acta* **58,** 2599–2608.

Hansen H. C. B., Koch C. B., Nanckekrogh H., Borggaard O. K., and Sorensen J. (1996) Abiotic nitrate reduction to ammonium—key role of green rust. *Env. Sci. Tech.* **30,** 2053–2056.

Hedin L. and Lundqvist S. (1969) Effects of electron-electron and electron-phonon interactions on the one-electron states of solids. *Solid State Phys.* **23,** 1–181.

Joyner R. W., Martin K. J., and Meehan P. (1987) Some applications of statistical tests in analysis of EXAFS and SEXAFS data. *J. Phys. C: Solid State Phys.* **20,** 4005–4012.

Kitahama K., Kiriyama R., and Baba Y. (1975) Refinement of the crystal structure of scorodite. *Acta Crysta.* **B31,** 322–324.

Livesey N. T. and Huang P. M. (1981) Adsorption of arsenate by soils and its relation to selected chemical-properties and anions. *Soil Sci.* **131,** 88–94.

Manceau A. (1995) The mechanism of anion adsorption on iron oxides: Evidence for the bonding of arsenate tetrahedra on free Fe(O,OH)6 edges. *Geochim. Cosmochim. Acta* **59,** 3647–3653.

Manning B. A., Fendorf S. E. and Goldberg S. (1998) Surface structures and stability of arsenic(III) on goethite: Spectroscopic evidence for inner-sphere complexes. *Env. Sci. Tech.* **32,** 2383–2388.

Masscheleyn P. H., Delaune R. D., and Patrick W. H. (1991) Effect of redox potential and pH on arsenic speciation and solubility in a contaminated soil. *Env. Sci. Tech.* **25,** 1414–1419.

Moore J. N., Ficklin W. H., and Johns C. (1988) Partitioning of arsenic and metals in reducing sediments. *Env. Sci. Tech.* **22,** 432–437.

Myneni S. C. B., Tokunaga T. K., and Brown G. E. Jr. (1997) Abiotic selenium redox transformations in the presence of Fe(II,III) oxides. *Science.* **278,** 1106–1109.

Newman A. C. D. (ed.) (1987) Chemistry of clays and clay minerals. In *Mineralogical Society Monograph 6.* p 480. John Wiley and Sons, New York.

Pierce M. L. and Moore C. B. (1982) Adsorption of arsenite and arsenate on amorphous iron hydroxide. *Water Res.* **16,** 1247–1253.

Schwertmann U. and Cornell R. M. (1991) Iron oxides in the laboratory: Preparation and characterization. VCH Publishers.

Schwertmann U. and Fechter H. (1994) The formation of green rust and its transformation to lepidocrocite. *Clay Min.* **29,** 87–92.

Shock, E.L., and Helgeson, H.C. (1988) Calculation of the thermodynamic and transport properties of of aqueous species at high pressures and temperatures: Correlation algorithims for ionic species and equation of state prediction to 5kb and 1000°C. *Geochim. Cosmochim. Acta* **52,** 2009–2036.

Stampfl P. P. (1969) Ein basisches eisen-(II)-(III) karbonat in rost. *Corr. Sci.* **9,** 185–187.

Sullivan K. A. and Aller R. C. (1996) Diagenetic cycling of arsenic in Amazon shelf sediments. *Geochim. Cosmochim. Acta* **60,** 1465–1477.

Sun X. H. and Doner H. E. (1996) An investigation of arsenate and arsenite bonding structures on goethite by FTIR. *Soil Science* **161,** 865–872.

Taylor R. M. (1973) Cyrstal structures of some double hydroxide minerals. *Min. Mag.* **39,** 377–389.

Trolard F., Genin J. M. R., Abdelmoula M., Bourrie G., Humbert B. and Herbillon A. (1997) Identification of a green rust mineral in a reductomorphic soil by mossbauer and raman spectroscopies. *Geochim. Cosmochim. Acta* **61,** 1107–1111.

Vins J., Subrt J., Zapletal V., and Hanousek F. (1987) Preparation and properties of green rust type substances. *Coll. Czech. Chem. Comm.* **52,** 93–102.

Waychunas G. A., Rea B. A., Fuller C. C., and Davis J. A. (1993) Surface chemistry of ferrihydrite. 1. EXAFS studies of the geometry

of coprecipitated and adsorbed arsenate. *Geochim. Cosmochim. Acta* **57,** 2251–2269.

Waychunas G. A., Davis J. A. and Fuller C. C. (1995) Geometry of sorbed arsenate on ferrihydrite and crystalline FeOOH: Re-evaluation of EXAFS results and topological factors in predicting sorbate geometry, and evidence for monodentate complexes. *Geochim. Cosmochim. Acta* **59,** 3655–3661.

Waychunas G. A., Fuller C. C., Rea B. A. and Davis J. A. (1996) Wide angle X-ray scattering (WAXS) of "two-line" ferrihydrite structure: Effect of arsenate sorption and counterion variation and comparison with EXAFS results. *Geochim. Cosmochim. Acta* **60,** 1765–1781.

White A. F. and Peterson M. L. (1996) Reduction of aqueous transition metal species on the surfaces of Fe(II)-containing oxides. *Geochim. Cosmochim. Acta* **60,** 3799–3814.